UDC 539.4

Creep-Fatigue Behavior Evaluation by Reversible Permeability of CrMo Ferritic Steel for Ultra-Supercritical Steem Power Plants

C. S. Kim

Department of Materials Science and Engineering, Chosun University, Gwangju, Republic of Korea

chs2865@chosun.ac.kr

The creep-fatigue of ferritic CrMo steel has been investigated by measuring the peak interval of the reversible magnetic permeability profile. The peak interval of reversible permeability was discussed in relation to the microstructural evolution during creep-fatigue. The peak interval decreased monotonously during creep-fatigue to $0.8N_f$ and increased thereafter. The decrease in the peak interval with increasing fatigue life fraction was related to the coarsening of fine precipitates and recovery of martensite laths. There is a strong linear relationship between the hardness and peak interval of reversible permeability.

Keywords: ferritic steel, fatigue, creep, degradation, permeability.

Introduction. Ferritic steels are key materials in fossil fuel and nuclear power plant components, such as boilers, steam pipes and steam turbines. The high chromium content of these steels increases their oxidation resistance; therefore, they can be utilised at higher temperatures than low alloy ferritic steels. These materials are developed in order to improve their properties. However, they are inevitably softened during the exposure to creep and fatigue at high temperatures [1–3]. Throughout the lifetime of a plant component, the structural material is exposed to various types of loading and temperatures. The extent of static or cyclic loading effects is normally taken into account during the design stage of the structural components. Generally, the interaction of various influences, such as cyclic loading and thermal history, can change the microstructure and mechanical properties upon occurring. In addition, desirable or undesirable states may occur during service That may influence the material state or behaviour. When the conventional destructive methods are at use, material properties changes cannot be detected in facilities during operation due to the fact that it is impossible to take specimens for microstructural examination and mechanical tests. Therefore, to ensure the integrity and service life of structural components, it is essential to understand their mechanical properties on a microstructural level. Many researchers have studied microstructural characterisation using some nondestructive evaluation techniques, such as acoustic, magnetic, electrical, and radiation methods [4–7]. However, the magnetic technique is sensitive to microstructural features, including grain boundaries, precipitates, voids, and dislocations, which are the principal microstructures contributing to the micromechanical properties of materials [8, 9]. The magnetic adaptive testing (MAT) was studied by Vértesy et al. with a purpose of comparison with Vickers hardness of cold rolled low-carbon steel. According to their report, the best linear relation with the Vickers hardness. Takahashi et al. investigated the relationship between mechanical and magnetic properties in cold rolled steel. They proposed a closed relation between the minor loop parameters and the rolling reduction of steel.

Recently, numerous studies have reported the fundamental physics of magnetic properties of materials in a research context. However, most reports and techniques may be inapplicable to damage characterisation in the industrial field due to limitations of specimen preparation and accessibility. The objective of this study is to examine the influence of creep-fatigue damage on reversible permeability in CrMo ferritic steel and to develop a nondestructive evaluation technique for damage characterisation.

1. **Experimental Procedure**. The chemical composition of CrMo ferritic steel used in this study is 0.09 C, 0.23 Si, 0.38 Mn, 0.015 P, 0.013 S, 0.065 Ni, 8.66 Cr, 0.9 Mo, 0.04 Cu, 0.21 V, 0.01 Al, 0.035 N, and 0.07 Nb by wt.%. The test materials were normalised at 1050℃ and air cooled, followed by tempering at 760℃. The creep-fatigue test was conducted at 550℃ under load control using a servo-hydraulic fatigue test machine with a resistance-heating furnace. The hold time at the maximum tensile stress was 600 s. Cylindrical specimens were prepared, with gauge length of 16 mm, diameter of 10 mm and shoulder radius of 20 mm. The microstructural observations were performed using field emission scanning electron microscopy (FESEM) after chemical etching with Vilella's reagent. In order to observe the dislocation substructures, thin foils were prepared using twin-jet polishing. Carbon replication was conducted in order to analyse the composition and structure of precipitates using transmission electron microscopy (TEM). The reversible permeability profile was obtained using a ferrite yoke probe.

The yoke probe was wound by pick-up coils: AC perturbing coils for modulating the magnetic field and DC magnetising coils for magnetizing the test specimens, as shown in Fig. 1. The specimen with a plate shape of 16 mm length, 5 mm width, and 1 mm thickness were magnetised by a maximum magnetic field of 12 kA/m with a sinusoidal waveform of 0.05 Hz. A perturbation field of 80 A/m was applied as a reference signal at 40 Hz. The induced first harmonic voltage in the pick-up coil was obtained using a lock-in amplifier. The reversible magnetic permeability (μ_r) is the limiting value of the incremental permeability when the alternating field strength approaches zero. According to Ryu et al., the most appropriate technique of analysis is measuring the peak interval calculated from reversible magnetic permeability [10].

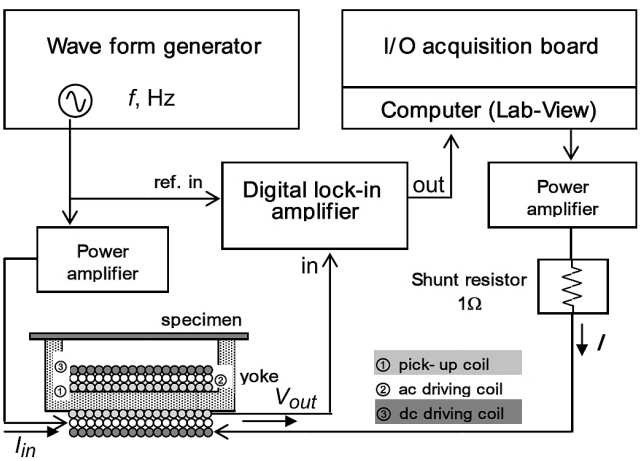

Fig. 1. Schematic diagram for the measurement of reversible magnetic permeability.

2. **Results and Discussion**. The as-tempered (i.e., normalised and tempered, NT) specimen exhibited a martensitic structure, containing a high dislocation density in the lath interior and fine precipitates on the prior austenite grain boundary (PAGB) and martensite lath boundary, as shown in Fig. 2. The PAG size was about 18 μm, and the width of the martensite lath was 0.21 μm. Figure 2a represents the typical precipitate morphologies observed by TEM, depicting tempered martensite, the triple point of PAGB and $Cr_{23}C_6$ precipitates on the PAGBs, as indicated by arrows. As observed by FESEM, well-developed laths could be clearly seen in Fig. 2b. All precipitates are in line with the lath boundaries. In Fig. 2c, the martensite lath structure is clearly seen to have elongated laths and tangled dislocations. The precipitates of 9Cr–1Mo ferritic steel play an important role in its mechanical properties. Extensive studies have shown two types of carbides, face

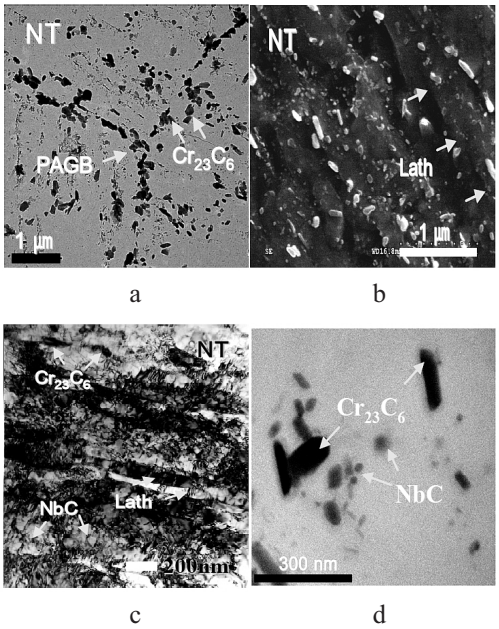

Fig. 2. TEM and FESEM micrographs of the as-tempered specimen: (a) TEM micrograph; (b) FESEM micrograph of lath; (c) TEM micrograph of lath boundaries; (d) TEM micrograph of $Cr_{23}C6$ and NbC precipitates.

centred cubic (fcc) $Cr_{23}C_6$ and (Nb,V)C, and the as-tempered state in CrMo ferritic steel, as shown in Fig. 2d.

Figure 3 represents the variation in peak interval of a symmetric double-humped curve of reversible permeability and Vicker's hardness as a function of the fatigue life fraction in creep-fatigue damaged CrMo ferritic steel. The peak interval of reversible permeability decreases during the creep-fatigue up to fracture. However, in the vicinity of the fracture region denoted by gray square symbol in Fig. 3, it increased by approximately 5.6% more than in the region far from the fracture. Due to coarsening of the fine precipitates and lath recovery, the peak interval of reversible permeability is monotonously decreased. However, the peak interval in near fracture region increases in the final failure as a result of the voids generated on the packet and PAGB.

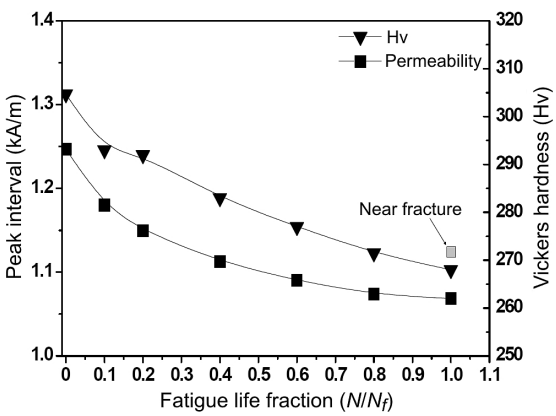

Fig. 3. Peak interval of reversible permeability and Vickers hardness as a function of the fatigue life fraction in creep-fatigue damaged CrMo ferritic steel.

Vickers hardness continuously decreased until failure, indicating softening. The variation in reversible permeability and hardness in increasing fatigue life fraction was related to the microstructural evolution during creep-fatigue, blocking the magnetic domain wall and dislocation motions. To understand its microstructural effects on permeability and hardness, microstructural evaluation of precipitates, dislocations, and martensite laths, was conducted at every stage of creep-fatigue using electron microscope analysis. There was a strong linear relationship between hardness (*Hv*) and peak interval (*PI*) of the reversible permeability with a correlation coefficient of 0.95 and the following empirical equation.

$$Hv = 76.5 + 184PI. \tag{1}$$

Figure 4 shows the FESEM and TEM micrographs. They represent the precipitate morphologies and dislocation substructures in creep-fatigue specimens at the maximum tensile hold time of 600 s. The $Cr_{23}C_6$ phase precipitates on the PAGB and the lath boundary were dominantly coarsened; therefore, the boundaries were unclear. The rapid coarsening of the precipitates on the PAGB indicated that these boundaries play an important part in the effective diffusion of solute atoms, such as Cr, Mo, and C. This implies a diffusion-controlled coarsening mechanism. Diffusion-controlled Ostwald ripening is expressed as $r^3 - r_0^3 = kt$, where r and r_0 are the average particle radius at times t and $t = 0$, respectively. The coarsening rate can be calculated by solving this equation for k. During creep-fatigue at 550°C, the coarsening rate of the $Cr_{23}C_6$ carbide for 600 s tensile hold times was approximately $4.4 \cdot 10^{-28}$ m^3/s. In contrast, the NbC phase is very stable at this testing temperature (e.g., $T_m = 1100$°C). The NbC precipitate size does not change during creep fatigue damage. The number of fatigue failures was 950 cycles for tensile hold times of 600 s.

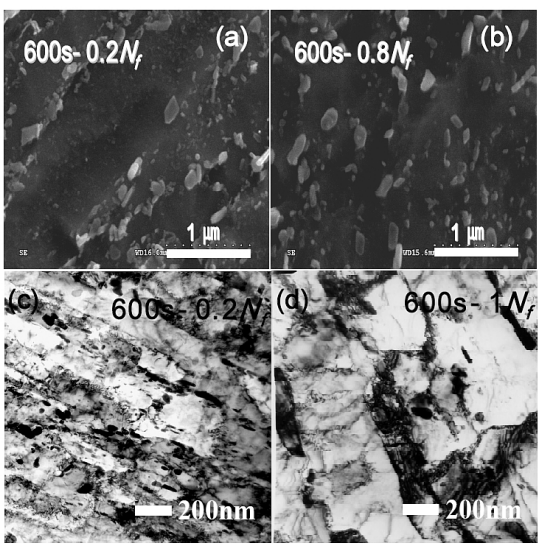

Fig. 4. FESEM (a, b) and TEM (c, d) micrographs showing precipitates and dislocation substructures of creep-fatigue damaged CrMo ferritic steel: (a) $0.2N_f$ at a hold time of 600 s; (b) $0.8N_f$ at a hold time of 600 s; (c) $0.2N_f$ at a hold time of 600 s; (d) N_f at a hold time of 600 s.

The precipitates grew slightly after fatigue failure. The total increase in the precipitates' average size was approximately 10% or less. The precipitates become effective pinning sites, which prevent domain-wall motion in relation to a periodic array of coherent precipitates with the matrix and have a close relationship with the volume fraction of the

precipitates [11]. In this study, the number of fine precipitates (i.e., $Cr_{23}C_6$) decreased with the fatigue life fraction due to the coarsening phenomenon resulting in a decrease in the peak interval of reversible permeability. Also, in this precipitate-hardened material, the fine precipitates, namely NbC and $Cr_{23}C_6$, are obstacles to the motion of the grain boundary, lath boundary and dislocation. However, loss of coherency (i.e., coherency strain) due to coarsening during creep-fatigue can strongly influence softening, (see Fig. 3). Figure 4c and 4d show typical TEM micrographs of the dislocation substructure in creep-fatigued specimens prepared using thin foils. The dislocation density in the martensite lath interior decreased with increasing creep-fatigue for both stress hold times. The as-tempered specimen showed many elongated martensite lath structures, as previously shown in Fig. 2c. There were high-density tangled dislocations within the martensite laths. Figure 4c and 4d show the typical microstructures of $0.2N_f$ and N_f at a hold time of 600 s. The lath width continuously grew during creep-fatigue, and the dislocation density within the lath interior was lower than that of the as-tempered specimen (see Fig. 4c). The lath width's growth is attributed to the recovery of dislocations and the lath boundaries' recombination. Grain boundaries influence the domain wall's motion via an effect related to the deflection of the magnetic moment existing along the grain boundaries. Coercivity is inversely proportional to grain diameter in materials where grain boundaries are the dominant obstacles to the domain wall's motion [12]. The peak interval of reversible permeability is two times the coercivity. However, the PAG size does not change during creep-fatigue. Only the subgrain (lath) size increased significantly after failure (see Fig. 4). This relationship between the magnetic coercivity and grain size is similar to the present result, which showed a decreasing peak interval as the martensite lath's width decreases. The peak interval of reversible permeability decreases monotonically due to coarsening of fine precipitates and lath recovery up to $0.8N_f$ of the fatigue life fraction. In contrast, the peak interval increases in the final failure as a result of the voids generated on the packet boundary and PAGB.

Conclusions. The peak interval of a symmetric double-humped curve of the reversible permeability reflects the microstructural effects on the domain wall motion. It is therefore closely related to the fine precipitates, dislocations, laths and void evolution during creep-fatigue damage. The peak interval of reversible permeability decreases monotonously due to coarsening of the fine precipitates and lath recovery. However, the increase in the vicinity of the fracture region was approximately 5.6% higher than that of the region far from the fracture due to void generation on the packet and PAGB. There is a strong linear relationship between the hardness and peak interval of the reversible permeability. Consequently, the peak interval of reversible permeability is a potential parameter, characterising creep-fatigue damage in fossil fuels and nuclear power materials.

Acknowledgments. This work was financially supported by the National Research Foundation of Korea (NRF) Grant funded by the Korean Government (NRF-2013M2A2A9043241).

1. F. Abe, T. Horiuch, M. Taneike, and K. Sawada, "Stabilization of martensitic microstructure in advanced 9Cr steel during creep at high temperature," *Mater. Sci. Eng. A*, **378**, 299–303 (2004).
2. C. S. Kim and I. K. Park, "Microstructural degradation assessment in pressure vessel steel by harmonic generation technique," *J. Nucl. Sci. Tech.*, **45**, 1036–1040 (2008).
3. Y. Wang, K. H. Mayer, A. Scholz, et al., "Development of new 11% Cr heat resistant ferritic steels with enhanced creep resistance for steam power plants with operating steam temperatures up to 650°C," *Mater. Sci. Eng. A*, **510-511**, 180–184 (2009).
4. C. S. Kim and C. J. Lissenden, "Precipitate contribution to the acoustic nonlinearity in nickel-based superalloy," *Chin. Phys. Lett.*, **26**, 086107 (2009).

5. H. Kikuchi, K. Ara, Y. Kamada, and S. Kobayashi, "Effect of microstructure changes on Barkhausen noise properties and hysteresis loop in cold rolled low carbon steel," *IEEE Trans. Magn.*, **45**, 2744–2747 (2009).
6. E. Schafler, M. Zehetbauer, A. Borbely, and T. Ungar, "'Dislocation densities and internal stresses in large strain cold worked pure iron," *Mater. Sci. Eng. A*, **234-236**, 445–448 (1997).
7. Y. Kiyanagi, T. Kamiyama, T. Nagata, et al., "Material characterization using cold neutron transmission spectroscopy," *Physica B: Condensed Matter*, **385-386**, 930–932 (2006).
8. G. Vértesy, I. Tomáš, S. Takahashi, et al., "Inspection of steel degradation by magnetic adaptive testing," *NDT & E Int.*, **41**, 252–57 (2008).
9. S. Takahashi, S. Kobayashi, H. Kikuchi, and Y. Kamada, "Relationship between mechanical and magnetic properties in cold rolled low carbon steel," *J. Appl. Phys.*, **100**, Issue 11, 113908-113908-6 (2006).
10. K. S. Ryu, C. S. Kim, U. B. Baek, and J. S. Lee, "Nondestructive evaluation for remanent life of aged 12Cr ferritic heat resisting steel by reversible permeability," *J. Magn. Magn. Mater.*, **326**, 257–260 (2013).
11. M. Taneike, F. Abe, and K. Sawada, "Creep strength of steel at high temperatures using nano-sized corbonitride dispersions," *Nature*, **424**, 294–296 (2003).
12. J. Degauque, B. Astie, J. L. Porteseil, and R. Vergne, "Influence of the grain size on the magnetic and magnetomechanical properties of high-purity iron," *J. Magn. Magn. Mater.*, **26**, 261–263 (1982).

Received 03. 08. 2015